ACS OMEGA

http://pubs.acs.org/journal/acsodf

Article

Construction of a Novel Substrate of Unfigured Islands-in-Sea Microfiber Synthetic Leather Based on Waste Collagen

Na Xu,* Yanan Tao, Xuechuan Wang, and Zijin Luo

Cite This: *ACS Omega* 2021, 6, 26086−26097

Read Online

ACCESS | Metrics & More | Article Recommendations

ABSTRACT: This study is to introduce waste collagen into an unfigured islands-in-sea microfiber nonwoven material, replacing the polyurethane impregnation section of the traditional manufacturing process with the collagen impregnation process. The modified collagen was first impregnated in polyamide/low-density polyethylene (PA/LDPE) fiber nonwoven to form a film. Then the low-density polyethylene component was extracted and dissolved in toluene, resulting in a collagen-based microfiber nonwoven substrate. Waste collagen was first modified to introduce C═C into the molecular chain to obtain vinyl collagen (CMA), and then the following film formation conditions for CMA were studied: 73% degree of substitution (DS), 3 h cross-linking time, and 0.005−0.01 wt % initiator concentration. Then, the preparation of CMA-PA/LDPE and toluene extraction processes were investigated. The optimum toluene extraction conditions were obtained as an extraction temperature of 85 °C and an extraction time of 110 min. The properties of the nonwoven materials were compared before (CMA-PA/LDPE) and after (PA-CMA) extraction. It was found that the homogeneity, tensile strength, and static moisture permeability of the PA-CMA materials prepared by CMA with 50 and 73% DS were all superior to those of PA/LDPE. In particular, the static moisture permeability of PA-CMA (691.6 mg/10 cm^2·24 h) increased by 36.2% compared to the microfiber synthetic leather substrate currently in the market. Using scanning electron microscopy (SEM), the continuity of a film of PA-CMA with 73% DS was observed to be better and the fibers were differentiated and relatively tighter fiber-to-fiber gap. The studied novel green process can eliminate the large amount of dimethylformamide (DMF) pollution caused by the current solvent-based polyurethane impregnation process.

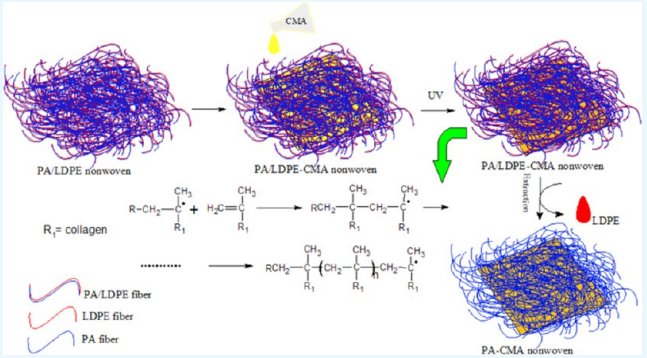

1. INTRODUCTION

The microfiber synthetic leather substrate is a composite material made of three-dimensional interwoven microfibers and a polyurethane (PU) filler with a microporous structure. The four key aspects of its manufacture include the manufacture of microfibers, the manufacture of high-density three-dimensional mesh nonwoven materials, the manufacture of open microporous-structured polyurethane films, and the surface layer manufacturing technology. This technology enables microfiber synthetic leather to mimic natural leather in terms of appearance, function, and sensibility.[1] This means that the structure of the original collagen fiber is simulated by the microfiber, and the three-dimensional nonwoven structure of the fiber simulates the woven form of the collagen fiber in natural leather so that the microfiber synthetic leather achieves a simulated effect in terms of microstructure, appearance, and texture, and physical properties. It has many properties and advantages of natural leather and is superior to natural leather in terms of mechanical strength, chemical resistance, homogeneity of quality, and adaptability to automated cutting and processing. However, compared to natural leather, its moisture absorption and permeability properties are poor and stifling to wear, so its moisture absorption and permeability properties need to be improved.[2−4] When analyzed structurally, the hydrophilic groups on the polyamide (PA) fibers and polyurethane filler in the base material are few and cannot match the number of hydrophilic groups on the collagen fibers in natural leather, which is one of the main reasons for the poor moisture absorption and permeability of the microfiber synthetic leather.

A series of studies[5−11] have been carried out to improve the moisture permeability of microfiber synthetic leather substrates, but the studies have focused mainly on modifying the surface of polyamide fibers by introducing a large number of

Received: June 10, 2021
Accepted: September 15, 2021
Published: September 28, 2021

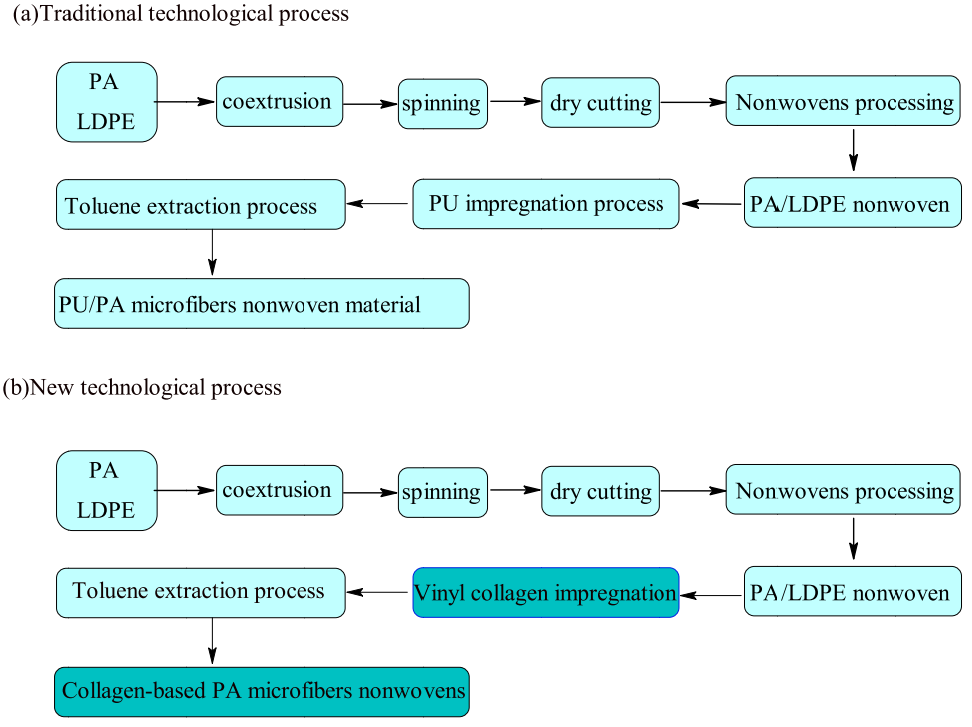

Figure 1. Traditional process (a) and novel process (b).

hydrophilic groups to improve the moisture absorption and permeability of the substrates. However, a few studies have been reported on modifications or substitution studies around polyurethane fillers. In this study, collagen was introduced into an unextracted unfigured islands-in-sea microfiber nonwoven system, a polyamide/low-density polyethylene (PA/LDPE) fiber nonwoven, to cross-link into a microporous film, replacing the polyurethane impregnation process in the traditional technological process (Figure 1). Then, the low-density polyethylene component was dissolved by the toluene extraction process to obtain a new collagen-based polyamide microfibers nonwoven (PA-vinyl collagen (CMA)) with high moisture absorption and permeability. This study used a green process method to replace the original polyurethane impregnation process with the collagen impregnation process, which can eliminate the large amount of dimethylformamide (DMF) pollution caused by the current solvent-based polyurethane impregnation process and greatly reduce environmental pollution.

2. RESULTS AND DISCUSSION

2.1. Optimum Preparation Conditions of CMA Membrane. The water solubility of CMA films with different degrees of substitution after soaking in water for 24 h is shown in Figure 2. In comparison, it was found that the CMA film with 0% degree of substitution (DS) was soluble in water, while all other CMA films were insoluble in water. In addition, all CMA films with DS greater than 73% almost sank to the bottom of water, indicating that the cross-linking degree increased and the film densities increased significantly.

Figure 3 shows the swelling and weight loss of CMA films in water for different DS values. As the degree of substitution of CMA increased, the swelling and weight loss of the film decreased after film formation. When the DS was greater than 73%, the swelling of the CMA film did not change much with

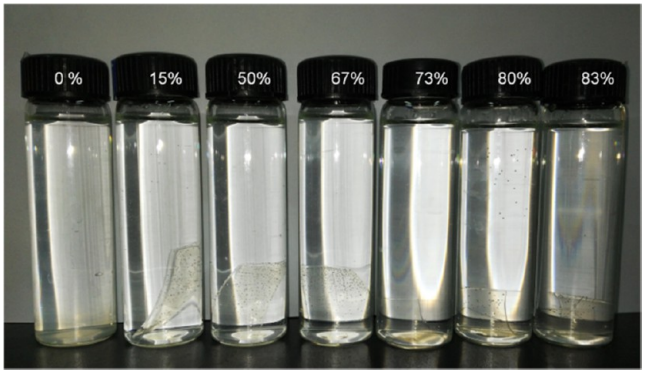

Figure 2. Water solubility of the CMA film after 24 h (room temperature).

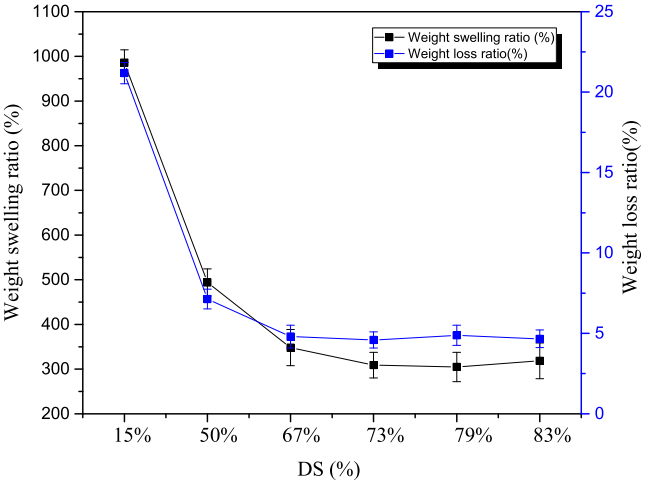

Figure 3. Effect of DS on the swelling and weight loss ratio of the CMA film.

https://doi.org/10.1021/acsomega.1c03061
ACS Omega 2021, 6, 26086−26097

the increase of the DS. When the DS was 73%, the swelling of the CMA film was the smallest. This may be due to the fact that the greater the DS of CMA, the greater the number of carbon−carbon double bonds (C ═ C), which would increase the number of cross-linking points per unit length and increase the cross-link densities. This should make the polymerization network too compact and dense, limiting the free swelling of the mesh and result in a lower swelling at the same time; with the increase of the cross-link densities of the CMA film, the weight loss rate was gradually reduced.

Figure 4 shows the effect of UV irradiation time on the swelling and weight loss of the CMA film. It can be observed

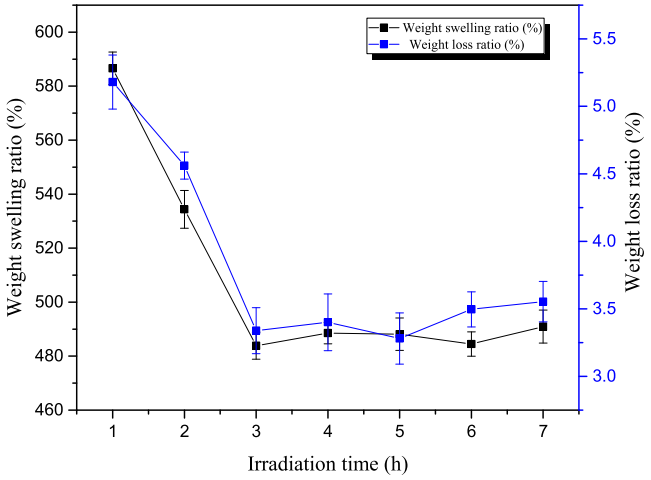

Figure 4. Effect of irradiation time on the swelling and weight loss of CMA films.

from Figure 4 that the swelling and weight loss of the CMA film gradually decreased with the increase of the UV irradiation time, and the swelling and weight loss of the CMA film did not change much when the UV irradiation time was more than 3 h. This indicated that when the irradiation time increased, the cross-link densities of CMA increased, resulting in a compact and dense polymeric CMA network structure (as shown in Figure 13), which limited the free swelling of the polymer mesh, thus leading to a decrease in swelling. At the same time, when the irradiation time increased the weight loss rate was reduced.

Figure 5 shows the relationship between the initiator concentration and the swelling of the CMA film. As the amount of initiator increased, the swelling and weight loss of the CMA film decreased, but when the initiator concentration was below 0.005−0.01% (by the mass of CMA solution), the swelling and weight loss of the resulting CMA film increased. This was probably because the initiator was the active center of the free radical polymerization reaction; when the initiator concentration was too low; due to the "cage effect",[12−18] the newly generated primary radicals did not fully react with the surrounding monomer molecules, which hindered the chain initiation, resulting in fewer cross-linking points per unit chain, and the resulting CMA film had a small cross-linking degree and the network structure was sparse. The resulting CMA film had a small cross-linking degree and the network was sparse and had a large mesh, which should freely expand in water and so the swelling degree was large. As the concentration of the initiator increased, the number of reactive radicals increased, which increased the initiation rate and allowed the polymer-

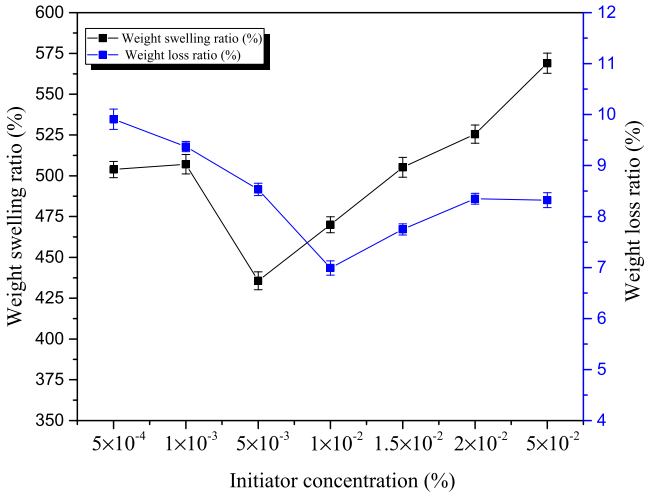

Figure 5. Effect of initiator concentration on weight swelling and weight loss ratio of the CMA film.

ization reaction to proceed more completely, resulting in a more cross-linked CMA film with a denser network structure and a smaller mesh size. However, when the initiator concentration continued to increase, the system was prone to "induced decomposition".[19−24] That is, the transfer of monomer radicals to the initiator caused the original radicals to terminate into stable macromolecules and consumed a new radical, resulting in a lower initiator efficiency, a lower cross-linking degree of the CMA film, and a looser polymer network, which increased the swelling in water. It was also found that as the initiator concentration increased, the weight loss of the CMA film in water decreased and then increased. Therefore, the initiator concentration of 0.005−0.01% (by the mass of CMA solution) was found to be the best for the initiation efficiency.

2.2. Optimum Extraction Conditions of LDPE in Nonwoven. Figure 6 shows the relationship between the extraction temperature and extraction rate for vinyl collagen with 15, 50, and 73% DS-impregnated PA/LDPE for a

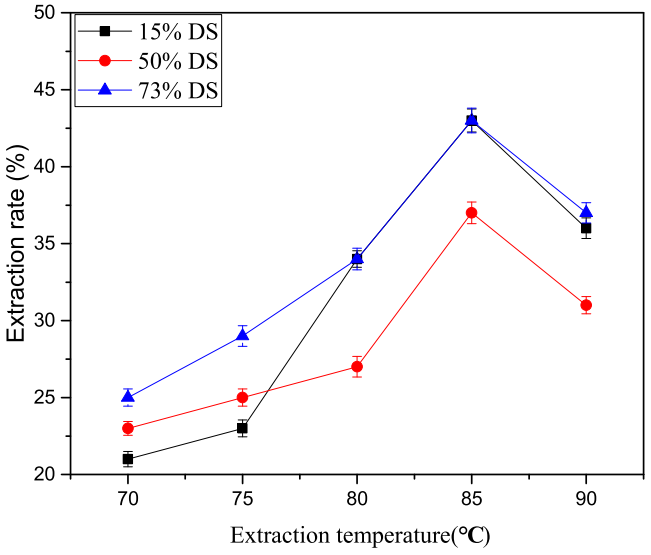

Figure 6. Effect of the extraction temperature of different samples on the extraction rate.

https://doi.org/10.1021/acsomega.1c03061
ACS Omega 2021, 6, 26086−26097

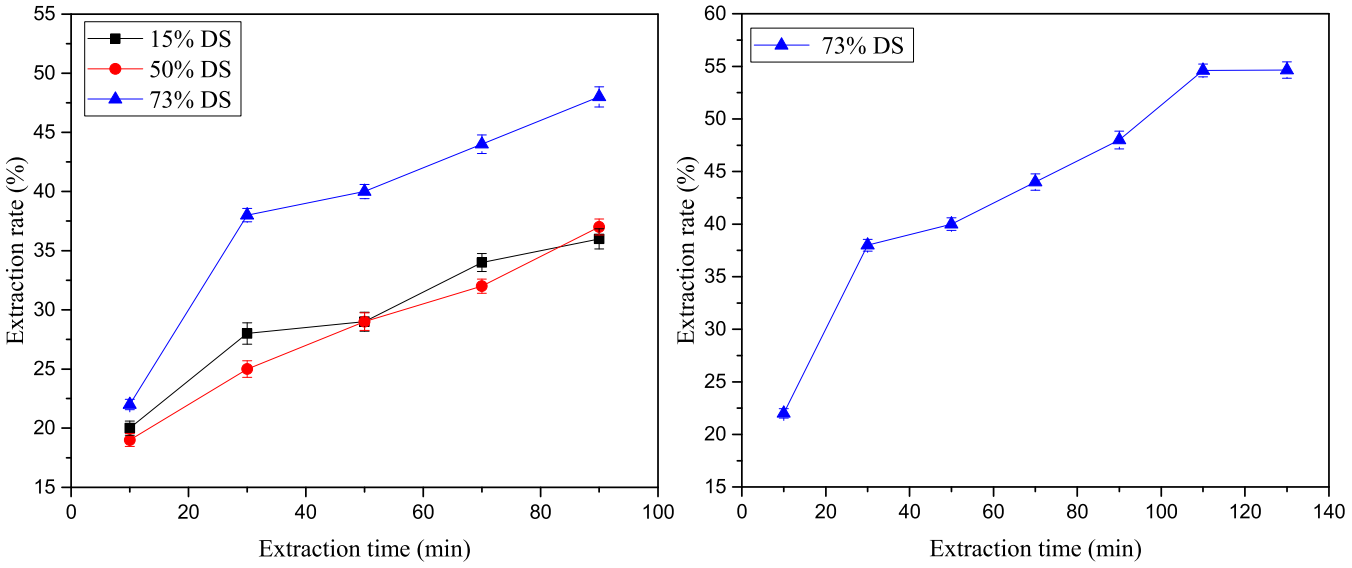

Figure 7. Effect of extraction time of different samples on the extraction rate.

constant extraction time of 1 h. From Figure 7, it can be seen that the optimum extraction temperature for the samples was 85 °C for 1 h. When the temperature was 75 °C, there was already a significant extraction effect and the extraction rate increased significantly with increasing time. As the temperature increased, the thermal movement of the toluene molecules was intensified and they better penetrated into the samples to dissolve the LDPE in the samples, while the diffusion of the LDPE into the hot toluene solution occurred. At higher temperatures, both the penetration of toluene and the thermal movement of the polyethylene molecular chains were enhanced, and the extraction rate increased significantly when 80−85 °C was reached.

Figure 7 shows the relationship between the extraction time and extraction rate for vinyl collagen with 15, 50, and 73% DS-impregnated PA/LDPE at an extraction temperature of 85 °C. The extraction rate of the different samples increased with increasing extraction time. Compared to vinyl collagen with 15 and 50% DS-impregnated samples, the vinyl collagen with 73% DS-impregnated PA/LDPE showed the best extraction results. The best extraction time for the samples was 110 min.

2.3. Physical Properties. Figure 8 shows the uniformity of the substrate before and after extraction of vinyl collagen-impregnated PA/LDPE nonwoven material with different DS values. It should be seen that when the DS values of vinyl collagen were 50 and 73%, the values of coefficient of variation (CV) values of the samples after extraction were 1.86 and 1.87% respectively, and the uniformity of the samples increased significantly after extraction (the CV values of the samples before extraction were 2.91 and 2.24%). When the DS of vinyl collagen was 15%, the CV values of the samples after extraction were increased (3.15%), indicating that the uniformity of the substrates decreased after extraction. It was inferred that, presumably, the film formation of the lower DS vinyl collagen in the nonwoven material was not very good, resulting in irregular fiber dispersion and no better fiber binding after extraction.

The analysis in Figure 9 shows that the tensile strength of PA/LDPE-CMA with different DS values of vinyl collagen was higher before extraction. The samples with 73% DS before extraction had the highest tensile strength, which was nearly

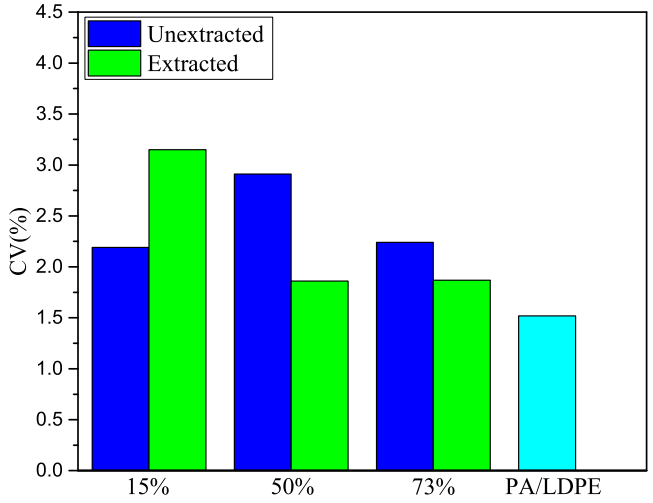

Figure 8. CV values of the thicknesses of different samples and PA/LDPE sample.

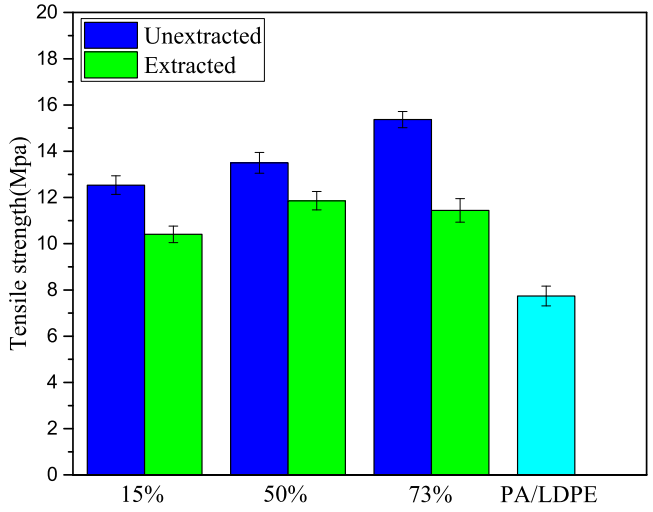

Figure 9. Tensile strength of different PA/LDPE samples before and after extraction.

https://doi.org/10.1021/acsomega.1c03061
ACS Omega 2021, 6, 26086−26097

double that of PA/LDPE. After extraction, the tensile strengths of PA-CMA with 50 and 73% DS were 11.86 and 11.44 MPa, respectively, both better than that with 15% DS (10.46 MPa) and PA/LDPE (7.74 MPa).

2.4. Moisture Permeability. From the analysis of the data in Figure 10, it can be seen that the static moisture permeability rate of the unextracted specimens was lower than that of the extracted specimens. Moreover, the static moisture permeability rates of samples with 50 and 73% DS after extraction were 691.6 mg/10 cm2·24 h and 625.7 mg/10 cm^2·24 h, respectively. The moisture permeability of samples with 50% after extraction increased by 36.2% compared to that of the figured islands-in-sea microfiber synthetic leather substrates (PA/PU) (the main microfiber synthetic leather substrate currently in the market).

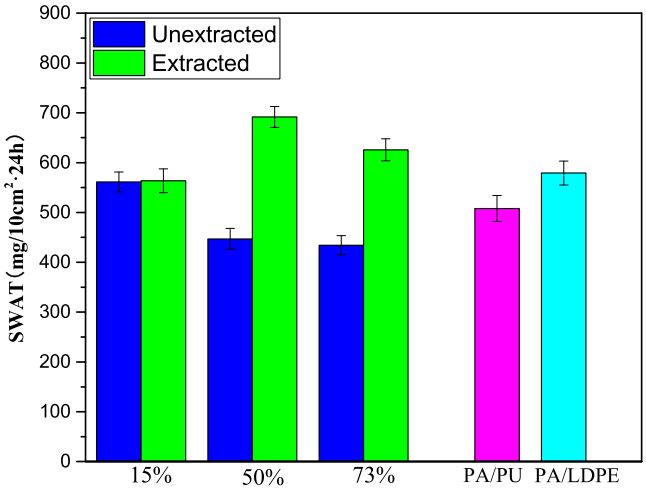

Figure 10. SWAT of different PA/PU and PA/LDPE samples before and after extraction.

2.5. Surface Topography and Morphology. Scanning electron microscopy (SEM) images of specimens of vinyl collagen with 73% DS before and after film formation were taken and are shown in Figure 11; the SEM photographs were obtained after the specimens had been sprayed by vacuum gold. The SEM images of vinyl collagen before and after UV cross-linking are shown in Figure 11. Vinyl collagen after UV cross-linking was found to have a distinct dense mesh structure, while the vinyl collagen without cross-linking showed a superimposed lamellar structure with no network. It was concluded that vinyl collagen formed a network structure after UV irradiation.

Environmental electron microscopy (ESEM) images of vinyl collagen membranes with different DS values are shown in Figure 12. Environmental scanning was used, i.e., vinyl collagen membranes of different DS values were allowed to undergo environmental scanning in a water-carrying environment and the resulting photographs are shown in Figure 12. In Figure 12a–f, vinyl collagen membranes with different DS values are shown ((a)–(f) show 15, 50, 67, 73, 79, and 83% DS respectively, with the same magnification 2000×). With 15% DS, the network structures of membranes are clearly seen with regular and uniform-sized pores, and with the increase of the substitution degree, the network structure became more and more dense.

Attenuated total reflection infrared (ATR-IR) spectroscopy of vinyl collagen membranes was performed. The infrared spectra of the vinyl collagen membranes before and after cross-linking were obtained and analyzed using a Vector-22 FTIR spectrometer (Bruker, Germany). From Figure 14, it can be seen that the uncross-linked vinyl collagen membranes exhibited peaks at 925 and 955 cm^{-1}. These were out-of-plane bending vibration peaks of hydrogen on the double-bonded carbon in the $RCH_3C{=}CH_2$ structure,[25−27] but all of these peaks disappeared after UV cross-linking, indicating that the carbon−carbon double bond was involved in the reaction during UV cross-linking.[28,29]

Figure 15 shows the horizontal SEM image of PA/LDPE-CMA with different DS values. It can be seen from Figure 15 that the film formation of PA/LDPE-CMA with 15% DS was poor, while that with 50 and 73% DS formed a more continuous film in the substrate and was interspersed and interlaced in the nonwoven fibers.

Figure 16 shows the SEM images of PA/LDPE impregnated with different degrees of substitution of vinyl collagen after extraction. The horizontal SEM image in (a) shows PA/LDPE nonwoven and (b) is PA nonwoven, in which LDPE is extracted by toluene. The cross-sectional SEM of (c) is still PA/LDPE nonwoven, and (d)−(f) are PA-CMA nonwoven with different DS values, in which LDPE is still extracted with toluene. It should be observed that the fibers of the extracted substrate are differentiated to some extent (as shown in Figure

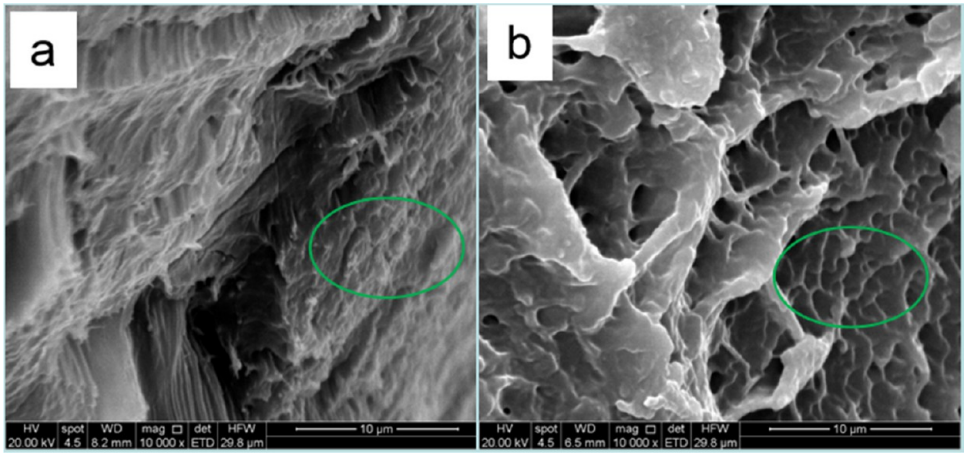

Figure 11. SEM images of the vinyl collagen film with 73% DS (a) before and (b) after cross-linking.

https://doi.org/10.1021/acsomega.1c03061
ACS Omega 2021, 6, 26086−26097

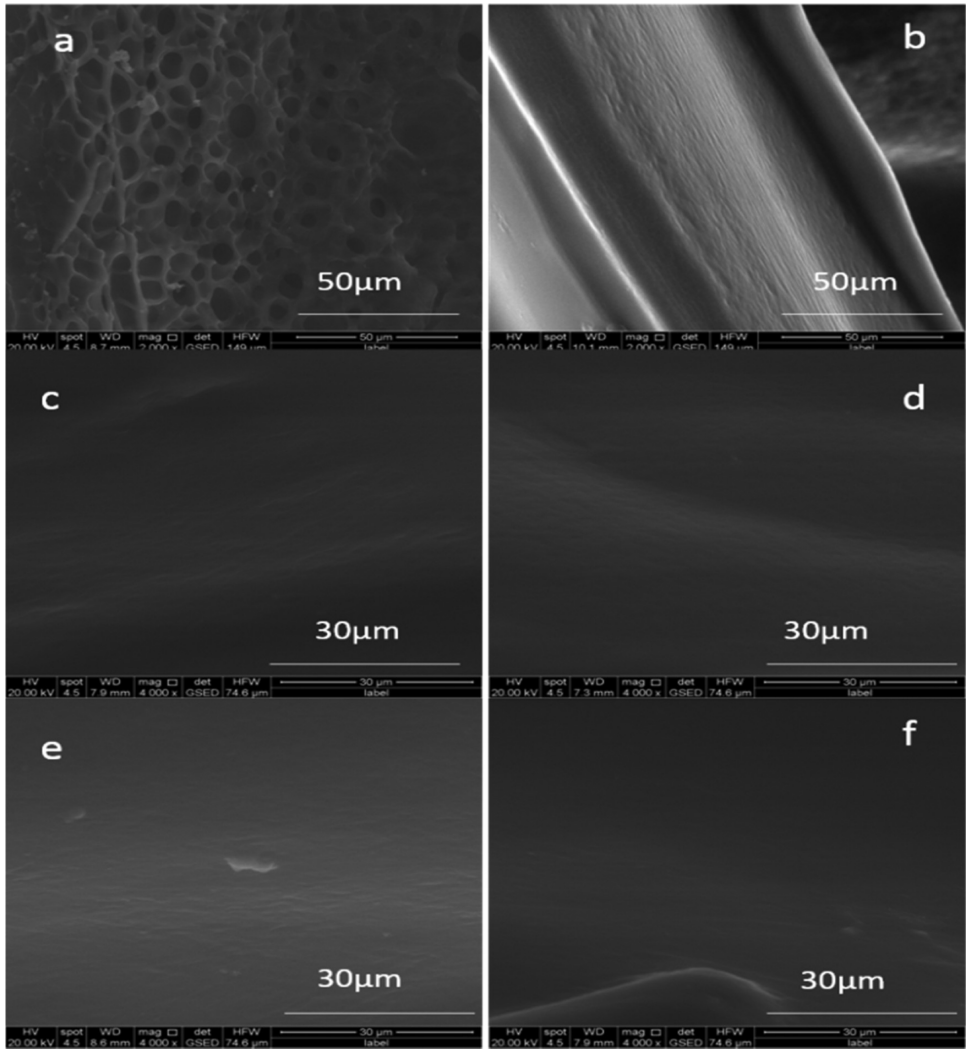

Figure 12. ESEM images of vinyl collagen membranes with different DS values ((a)−(f): 15, 50, 67, 73, 79, and 83% DS, respectively).

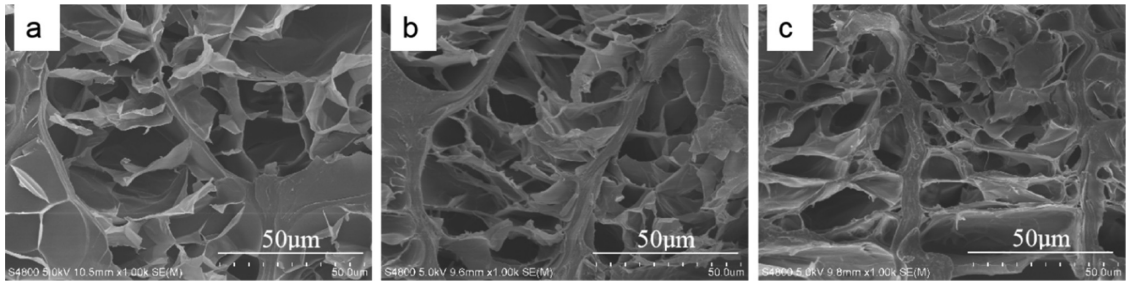

Figure 13. SEM images of vinyl collagen membranes with different UV irradiation times ((a)−(c): 1−3 h respectively), by freeze-drying after soaking in water for 24 h.

16b,d−f). Furthermore, the fiber-to-fiber gap in the collagen-impregnated substrates becomes tighter than in the non-collagen-impregnated PA/LDPE material. The degree of compactness increased with the degree of substitution of vinyl collagen, and PA-CMA with 73% DS vinyl collagen impregnation was the most compact.

3. CONCLUSIONS

In this study, collagen was introduced into a polyamide/low-density polyethylene (PA/LDPE) fiber nonwoven, to cross-link into a microporous film, replacing the polyurethane impregnation process in the traditional technological process (as shown in Figure 1). The static moisture permeability rate of the PA-CMA material with 50% DS was 691.6 mg/10 cm^2·24 h, an increase of 36.2% over the current mainstream microfiber synthetic leather substrate (PA/PU). This specific application can eliminate the large amount of DMF pollution caused by the polyurethane impregnation process of the traditional process and greatly reduce environmental pollution. Due to the presence of collagen, the final product, collagen-based nonwoven PA microfiber has excellent moisture absorption and comfortable wear performance. The cost of

https://doi.org/10.1021/acsomega.1c03061
ACS Omega 2021, 6, 26086−26097

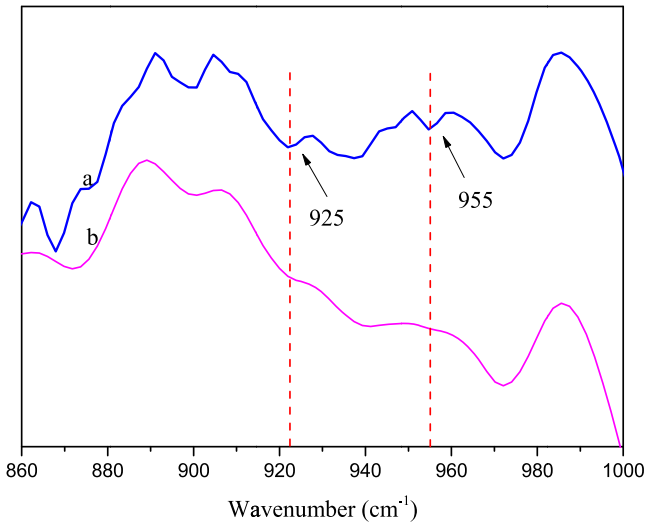

Figure 14. ATR-IR spectra of vinyl collagen before and after cross-linking ((a) uncross-linked and (b) cross-linked).

this innovative process is very low. Because the collagen used comes from the waste collagen resources produced in the leather industry, at the same time, this process does not use DMF, which eliminates the cost of DMF environmental management.

4. MATERIALS AND METHODS

The collagen used in this study was acquired from Xueyang Gelatin Factory (Hebei, China). The indefinite island microfiber nonwoven (PA/LDPE, 1.4 mm) was acquired from Shandong Huada Group Co. (Shan dong, China). The photoinitiator (Irgacure 2959) was acquired from BASF. Methacrylic anhydride (GR) was purchased from Adamas Reagents Ltd. Methylbenzene was purchased from Tianjin Tianli Chemical Reagent Co.

Vinyl collagen (CMA) was prepared by the reaction of collagen with methacrylic anhydride by a process adapted from the methodology reported in ref 30. Briefly, 5 g of collagen was weighed and dissolved in a corked conical flask containing 50 mL of phosphate-buffered saline (pH 7.4). The stoppered conical flask was placed in a constant temperature water bath at 70 °C with constant stirring for about 30 min. The temperature of the fully dissolved collagen solution was lowered to a suitable reaction temperature, and after the temperature became constant a certain amount of methacrylic anhydride was slowly added dropwise to the above conical flask at a rate of 1 mL/min. After reacting for a certain time, the resulting CMA solution was placed in a dialysis bag with 3500 Da molecular weight cutoff (MWCO) and dialyzed at 40 °C for 24 h. The dialyzed CMA solution was freeze-dried and then refrigerated at 5 °C.

4.1. Preparation of Vinyl Collagen Membranes. A solution of vinyl collagen with 15, 50, 69, 73, 79, and 83% DS (the collagen solution had a mass of approximately 50 g and a

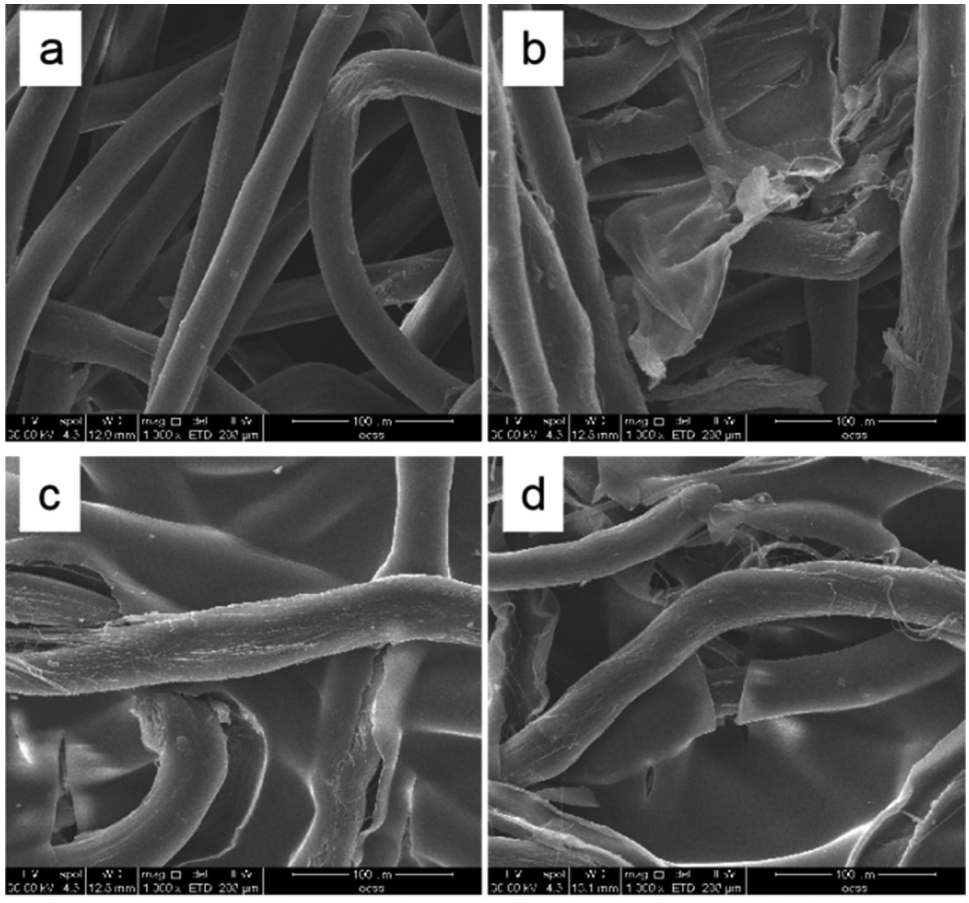

Figure 15. Horizontal SEM images of PA/LDPE-CMA with different DS values ((a) PA/LDPE, (b) 15% DS, (c) 50% DS, (d) 73% DS).

https://doi.org/10.1021/acsomega.1c03061
ACS Omega 2021, 6, 26086−26097

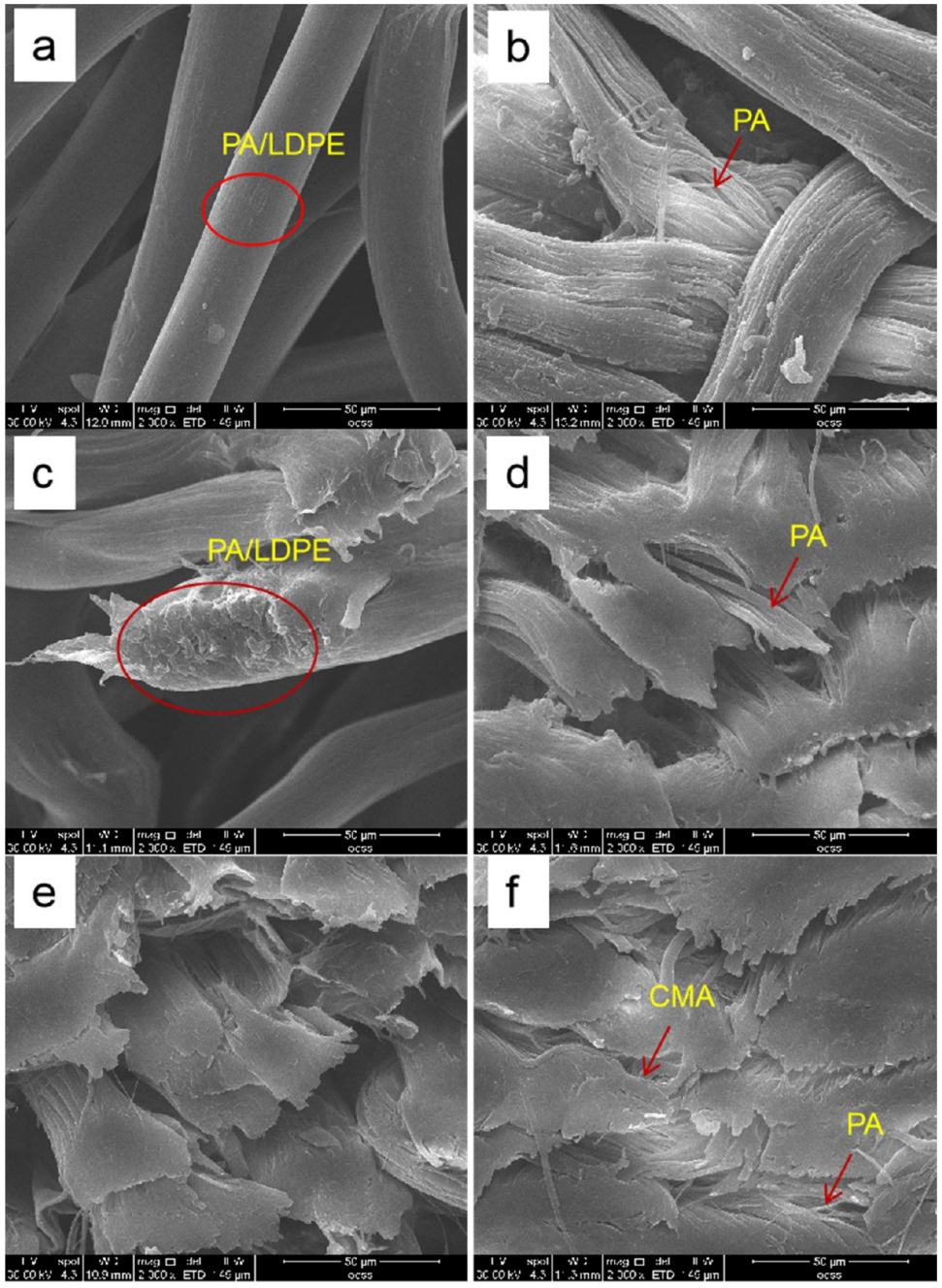

Figure 16. SEM images of (a) horizontal PA/LDPE, (b) PA, (c) PA/LDPE, (d) PA-CMA,15% DS, (e) PA-CMA, 50% DS, and (f) PA-CMA, 73% DS.

solid content of 6 wt %) was added to a UV initiator (Irgacure 2959) with initiator concentrations of 0.0005, 0.001, 0.005, 0.01, 0.015, 0.02, and 0.05 wt % respectively. After mixing well by ultrasonic shaking, they were poured directly into the molds of PTFE and then placed in a UV cross-linker for light irradiation for 1−7 h before being removed and left to dry naturally.

4.2. Collagen-Impregnated PA/LDPE Nonwoven Materials. PA/LDPE was cut into samples using a 55 cm diameter disc sampler, washed with hot water at 40 °C for 30 min, removed every 10 min and rolled on a small rolling mill at a pressure of 1.5 MPa Then they were washed to remove impurities, dried naturally, weighed and its mass was recorded (PA/LDPE).

The vinyl collagen (CMA) solutions made with 73, 50, and 15% DS were taken (50 ± 2 g) (solid content of 6 ± 0.5 wt %), added with 0.0025 wt % UV initiator (Irgacure 2959), and mixed well. The reason was that the greater the DS of CMA, the greater the number of carbon−carbon double bonds (C═C). This increased the number of cross-linking points per unit length and the cross-link densities (as shown in Figure 17), which made the polymerization network compact and dense (as shown in Figure 12) and insoluble in water (as shown in Figure 2). So, the 73, 50, and 15% DS of vinyl collagen were selected for contrastive research. Afterward, the pretreated PA/LDPE specimens were placed in a beaker containing the mixed vinyl collagen solution and dispersed by ultrasonic shaking for 30 min to ensure that the collagen solution could fully

https://doi.org/10.1021/acsomega.1c03061
ACS Omega 2021, 6, 26086−26097

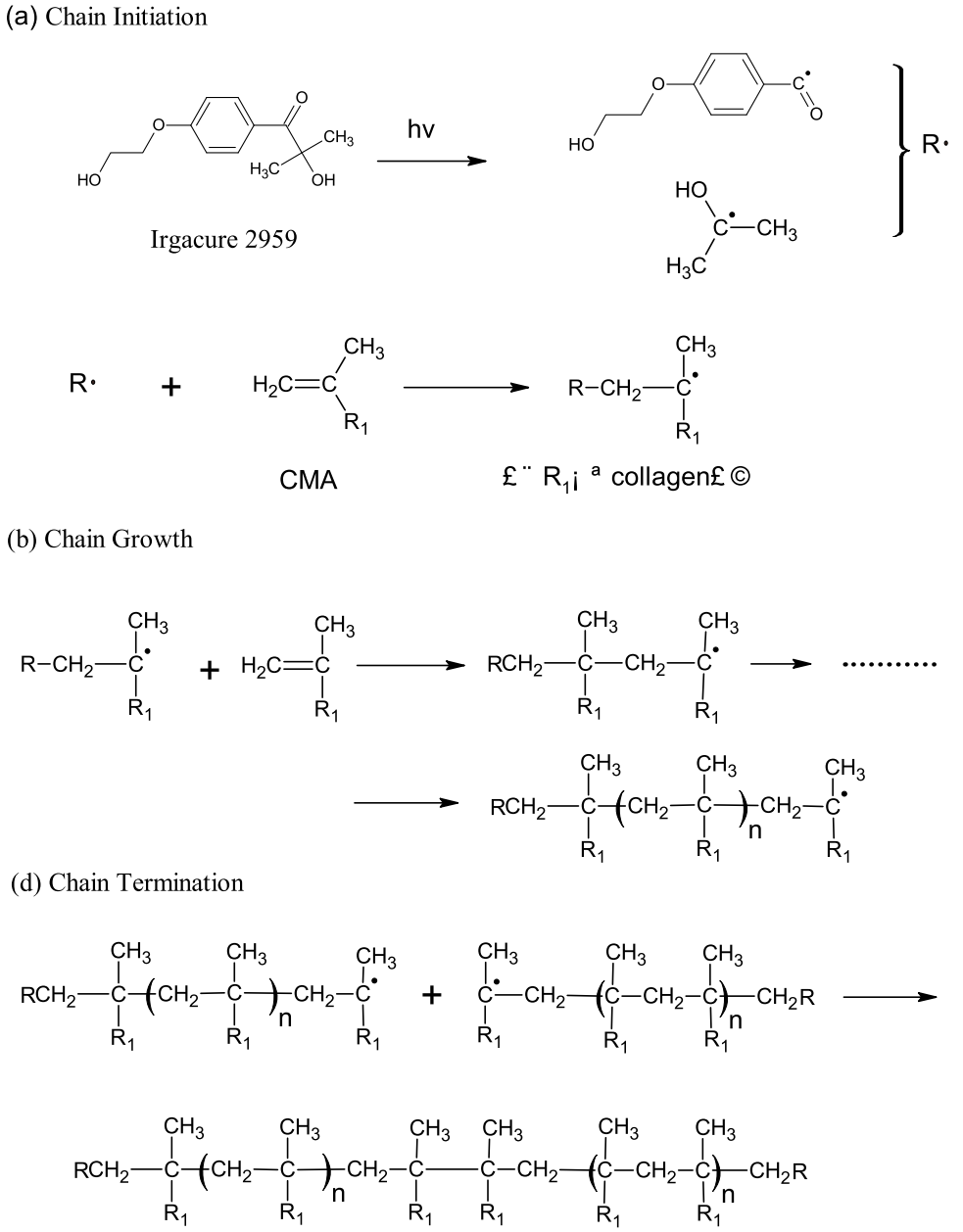

Figure 17. Cross-linking polymerization mechanism of ultraviolet initiated CMA.

impregnate the PA/LDPE. The collagen-impregnated PA/LDPE specimens were removed and placed in a UV cross-linker (50 W, 365 nm, exposure chamber size 34 cm × 26 cm × 15 cm, the irradiation distance: 15 cm). The collagen/PA/LDPE composite (PA/LDPE-CMA) was obtained by natural drying after 3 h of irradiation, weighed, and the mass was recorded.

4.3. Preparation of PA-CMA Composites. Toluene (100 mL) was placed in five stainless steel cups and preheated in a constant temperature water bath at 70, 75, 80, 85, and 90 °C. The PA/LDPE-CMA specimens were then extracted in the preheated toluene for 10, 30, 50, 70, and 90 min. The samples were washed with DMF and then rinsed in running water and dried to produce collagen/polyamide microfiber composites (PA-CMA) (as shown in Figure 18). Three parallel experiments were carried out for each group of experiments.

4.4. Performance Testing. For swelling characterization,[31−38] the prepared vinyl collagen film was cut into 2.5 cm × 1.5 cm specimens and dried at 80 °C for 2 h to obtain m_1. Then the film was soaked in 35 mL of distilled water for 24 h and the surface water was removed with filter and weighed to obtain m_2. After removing the surface water of the collagen film, the film was dried at 80 °C for 2 h to obtain m_3.

$$S = \frac{(m_2 - m_1)}{m_1} \times 100\% \quad (1)$$

where m_1 is the mass of the specimen before swelling and m_2 is the mass of the specimen after 24 h of swelling (after floating water has been removed from the surface).

The mass swelling ratio (%) was calculated using formula 1. The weight loss rate (%) was calculated by formula 2.

https://doi.org/10.1021/acsomega.1c03061
ACS Omega 2021, 6, 26086−26097

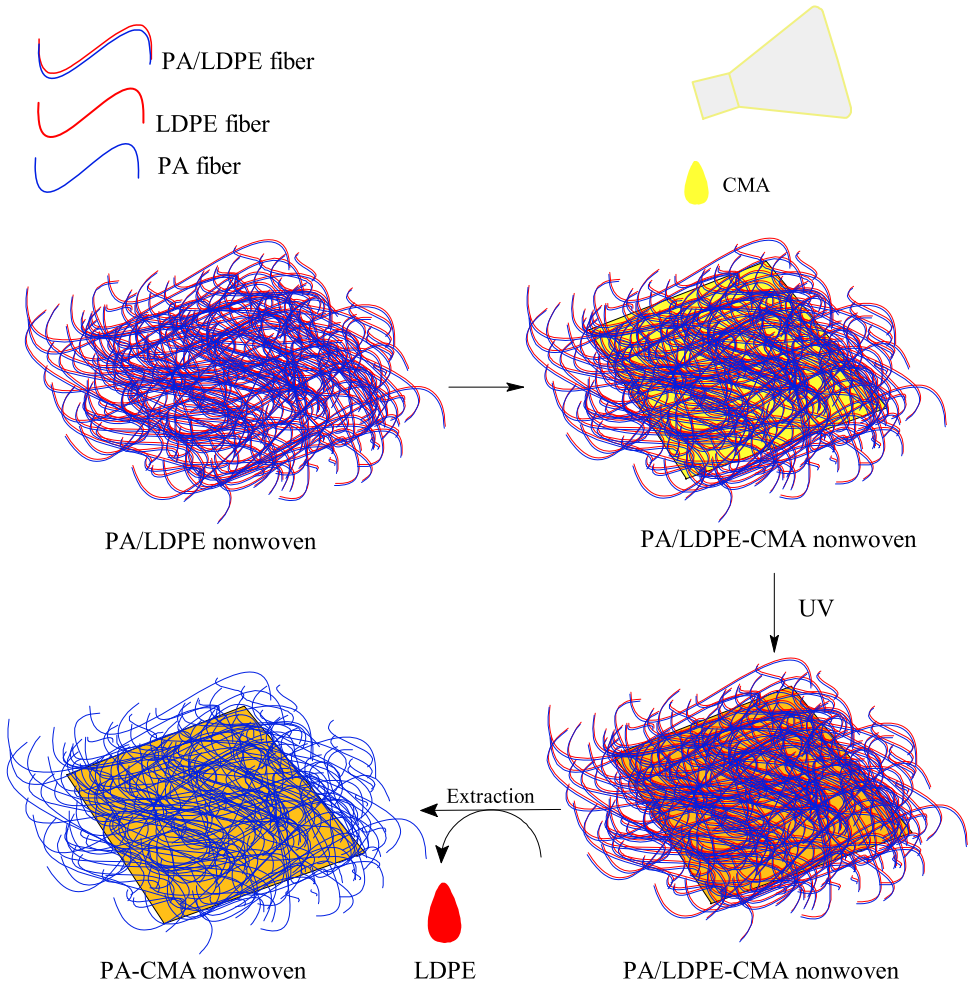

Figure 18. Schematic diagram of the preparation process of PA-CMA.

$$W = \frac{(m_3 - m_1)}{m_1} \times 100\% \quad (2)$$

where m_1 is the mass of the specimen before swelling and m_3 is the mass after drying in an oven at 80 °C for 2 h.

The extraction rate was calculated by formula 3. Naturally dried PA/LDPE specimens were accurately weighed to obtain mass m_a and mass m_b was recorded for PA/LDPE-CMA specimens. PA/LDPE-CMA specimens were placed in preheated toluene in a stainless steel cup at approx. 85 °C and extracted separately to obtain PA-CMA, which was dried, and weighed accurately to obtain mass m_c.

$$\text{extraction rate} = \frac{m_c - m_b}{m_a} \times 100\% \quad (3)$$

where, m_a is the mass of PA/LDPE, m_b is the mass of the PA/LDPE-CMA specimen, and m_c is the mass of PA-CMA after extraction.

The thickness was determined by ISO 2589:2016[39] at 10 different points randomly on the specimens and the average value was calculated. The coefficient of variation (CV) of the thickness was calculated.

Tensile strength was the degree of force applied to a specimen when it was stretched at a certain rate until it was broken. In accordance with ISO 3376:2020,[40] a medium-sized specimen was used in the experiment. A tensile machine with a speed of 100 mm/min was used for testing, the load value was recorded, and the tensile strength was calculated according to eq 3

$$T = \frac{P}{S} \quad (4)$$

where T is tensile strength (N/mm^2 or Maps), P is the maximum force at break of specimen (N), and S is cross-sectional area at the breakpoint (mm^2).

4.5. Characterization. Scanning electron microscopy (SEM) was performed before and after cross-linking of vinyl collagen, while observing the microscopic morphological changes in the composite before and after extraction. The specimens were observed after vacuum spraying the alloy using an FEIQ45 + EDAX Octane Prime environmental scanning electron microscope (FEI) and energy dispersive X-ray analysis (EDAX) was performed at an accelerating voltage of 20 kV.

Environmental scanning electron microscopy (ESEM) was performed to observe the vinyl collagen membranes with different degrees of substitution in the water-carrying state after cross-linking using the FEIQ45 + EDAX Octane Prime environmental scanning electron microscope (FEI) and EDAX. Ambient scanning observation conditions were as follows: a temperature of 5 °C, 50% humidity, and 438 Pa air pressure.

Attenuated total reflection infrared spectroscopy (ATR-IR) was performed to obtain and analyze the infrared spectra of vinyl collagen before and after cross-linking using a VECTOR-

https://doi.org/10.1021/acsomega.1c03061
ACS Omega 2021, 6, 26086−26097

22 FTIR spectrometer (Bruker, Germany) in the range of 400−4000 cm^{-1}.

AUTHOR INFORMATION

Corresponding Author

Na Xu − *College of Bioresources Engineering Chemical and Materials Engineering, Shaanxi University of Science and Technology, Xi'an, Shaanxi 710021, China;* orcid.org/0000-0002-2582-1011; Email: xuna19992003@163.com

Authors

Yanan Tao − *College of Bioresources Engineering Chemical and Materials Engineering, Shaanxi University of Science and Technology, Xi'an, Shaanxi 710021, China*

Xuechuan Wang − *College of Bioresources Engineering Chemical and Materials Engineering, Shaanxi University of Science and Technology, Xi'an, Shaanxi 710021, China*

Zijin Luo − *College of Bioresources Engineering Chemical and Materials Engineering, Shaanxi University of Science and Technology, Xi'an, Shaanxi 710021, China*

Complete contact information is available at: https://pubs.acs.org/10.1021/acsomega.1c03061

Funding

This work was supported by the National Natural Science Foundation of China (Grant No. 21808136), the National Key R&D Program of China (Grant No. 2017YFB0308500), the Key Scientific Research Group of Shaanxi Province (Grant No. 2020TD-009), the Key Scientific Research Program of Shaanxi Provincial Department (Collaborative Innovation Center Project) (20JY003), and the Youth Innovation Team of Shaanxi Universities.

Notes

The authors declare no competing financial interest.

ACKNOWLEDGMENTS

The author acknowledges the National Natural Science Foundation and College of Bioresources Engineering Chemical and Materials Engineering, Shaanxi University of Science and Technology.

REFERENCES

(1) Duo, Y. C.; Qian, X. M.; Zhao, B. B.; Qian, Y.; Xu, P.; Qi, J. J. Micro/nano microfiber synthetic leather base with different nanofiber diameters. *J. Ind. Text.* **2021**, *50*, 1127−1142.

(2) Zhao, B. B.; Qian, X. M.; Qian, Y.; Fan, J. T.; Feng, Y.; Duo, Y. C.; Zhang, H. Preparation of high-performance microfiber synthetic leather base using thermoplastic polyurethane/sulfonated polysulfone electrospun nanofibers. *Text. Res. J.* **2019**, *89*, 2813−2820.

(3) Xu, N.; Wang, X. C.; Wang, L. Z.; Zheng, Y. G.; Zhang, F. J.; Guo, P. Y. Modification of PA/PU superfine non-woven fiber for "breath" property using collagen and vegetable tannins. *J. Ind. Text.* **2019**, *48*, 1593−1615.

(4) Wang, X. C.; Xu, N.; Guo, P. Y.; Wang, Q. Improving moisture absorbent and transfer abilities by modifying superfine fiber synthetic leather base with collagen-chrome tannins. *Text. Res. J.* **2016**, *86*, 765−775.

(5) Ren, L. F.; Ma, X. D.; Wang, S. T.; Qiang, T. T. Surface modification of bundle-type polyamide fiber nonwoven with collagen to improve its hydrophilicity. *J. Ind. Eng. Chem.* **2020**, *89*, 392−399.

(6) Qiang, T. T.; Wang, Y. Y.; Wang, L. Z.; Zheng, Y. G.; Zhang, F. J.; Zheng, S. J. Study on the effect of the sanitary properties of microfiber synthetic leather base by using a filling agent. *Text. Res. J.* **2018**, *88*, 1437−1449.

(7) Qiang, T. T.; Wang, X. Q.; Wang, X. C.; Ren, L. F.; Guo, P. Y. Study on the improvement of water vapor permeability and moisture absorption of microfiber synthetic leather base by collagen. *Text. Res. J.* **2015**, *85*, 1394−1403.

(8) Ren, L. F.; Wang, N.; Sun, S.; Qiang, T. T.; Wang, X. C. Improvement of the Sanitary Property of Microfiber Synthetic Leather Base by PAMAM. *J. Eng. Fibers Fabr.* **2015**, *10*, 40−46.

(9) Wang, X. C.; Wang, X. Q.; Qiang, T. T.; Ren, L. F.; Wang, P. Y. Modification of Microfiber Synthetic Leather Base and Model by Collagen. *J. Eng. Fibers Fabr.* **2015**, *10*, 78−84.

(10) Ren, L. F.; Zhao, G. H.; Wang, X. C.; Qiang, T. T.; Wang, N.; Han, C. Hygienic Property of Microfiber Synthetic Leather Base Modified via a "Two-Step Method". *J. Eng. Fiber. Fabr.* **2014**, *9*, 36−49.

(11) Ren, L. F.; Zhao, G. H.; Qiang, T. T.; Wang, X. C.; Wang, N. Synthesis of amino-terminated hyperbranched polymers and their application in microfiber synthetic leather base dyeing. *Text. Res. J.* **2013**, *83*, 381−395.

(12) Alili, A. S.; Siddiquee, M. N.; Klerk, A. D. Origin of Free Radical Persistence in Asphaltenes: Cage Effect and Steric Protection. *Energy Fuels* **2020**, *34*, 348−359.

(13) Barry, J. T.; Berg, D. J.; Tyler, D. R. Radical Cage Effects: The Prediction of Radical Cage Pair Recombination Efficiencies Using Microviscosity Across a Range of Solvent Types. *J. Am. Chem. Soc.* **2017**, *139*, 14399−14405.

(14) Yago, T.; Wakasa, M. Nanoscale Structure of Ionic Liquid and Diffusion Process as Studied by the MFE Probe. *J. Phys. Chem. C* **2011**, *115*, 2673−2678.

(15) Zhang, H.; Yu, K.; Cayre, O. J.; Harbottle, D. Interfacial particle dynamics: One and two step yielding in colloidal glass. *Langmuir* **2016**, *32*, 13472−13481.

(16) Kopinke, F. D.; Georgi, A. What Controls Selectivity of Hydroxyl Radicals in Aqueous Solution-Indications for a Cage Effect. *J. Phys. Chem. A* **2017**, *121*, 7947−7955.

(17) Barry, J. T.; Berg, D. J.; Tyler, D. R. Radical Cage Effects: Comparison of Solvent Bulk Viscosity and Microviscosity in Predicting the Recombination Efficiencies of Radical Cage Pairs. *J. Am. Chem. Soc.* **2016**, *138*, 9389−9392.

(18) Male, J. L.; Lindfors, B. E.; Covert, K. J.; Tyler, D. R. The Effect of Radical Size and Mass on the Cage Recombination Efficiency of Photochemically Generated Radical Cage Pairs. *J. Am. Chem. Soc.* **1998**, *120*, 13176−13186.

(19) Tanimura, M.; Watanabe, N.; Ijuin, H. K.; Matsumoto, M. Intramolecular charge-transfer-induced decomposition promoted by an aprotic polar solvent for bicyclic dioxetanes bearing a 4-(benzothiazol-2-yl)-3-hydroxyphenyl moiety. *J. Org. Chem.* **2011**, *76*, 902−8.

(20) Tseng, J. M.; Lin, Y. F. Evaluation of a tert-Butyl Peroxybenzoate Runaway Reaction by Five Kinetic Models. *Ind. Eng. Chem. Res.* **2011**, *50*, 4783−4787.

(21) Khelifa, F.; Ershov, S.; Habibi, Y.; Snyders, R.; Dubois, P. Free-Radical-Induced Grafting from Plasma Polymer Surfaces. *Chem. Rev.* **2016**, *116*, 3975−4005.

(22) El Harfi, J.; Kingman, S. W.; Dimitrakis, G.; Robinson, J. P.; Irvine, D. J. Dielectric properties of free radical initiators-investigation of thermal decomposition products. *Ind. Eng. Chem. Res.* **2012**, *51*, 15811−15820.

(23) Dumont, Q.; Barcenas, M.; Dossmann, H.; Bailloux, I.; Buisson, C.; Mechin, N.; Molina, A.; Lasne, F.; Rannulu, N. S.; Cole, R. B. Improved Steroids Detection and Evidence for Their Regiospecific Decompositions Using Anion Attachment Mass Spectrometry. *Anal. Chem.* **2016**, *88*, 3585−3591.

(24) He, F.; Xia, N.; Zheng, Y.; Fan, H.; Hu, X.; et al. Boosting Oxygen Electroreduction over Strained Silver. *ACS Appl. Mater. Interfaces* **2020**, *12*, 57134−57140.

(25) Wilkosz, N.; Czaja, M.; Seweryn, S.; Skirlinska-Nosek, K.; Szymonski, M.; Lipiec, E.; Sofinska, K. Molecular Spectroscopic Markers of Abnormal Protein Aggregation. *Molecules* **2020**, *25*, 2498.

(26) Barth, A. Infrared spectroscopy of proteins. *Biochim. Biophys. Acta, Bioenerg.* **2007**, *1767*, 1073−1101.
(27) Blum, M. M.; John, H. Historical perspective and modern applications of Attenuated Total Reflectance-Fourier Transform Infrared Spectroscopy (ATR-FTIR). *Drug Test. Anal.* **2012**, *4*, 298−302.
(28) Bracker, R.; Dominguez, K.; Anthony, S. Analytical Methods for Monitoring the Degradation of Plasmonic Nanoparticles in Solution: An Instrumental Analysis Laboratory Exercise. *J. Chem. Educ.* **2020**, *97*, 1151−1156.
(29) Purvis, K.; Cisek, R.; Tokarz, D. New Activity for Instrumental Analysis: Laser Beam Profiling. *J. Chem. Educ.* **2019**, *96*, 1977−1981.
(30) Xu, N.; Wang, X. C.; Ren, L. F.; Ma, X. D.; Shi, Y. Y. Study of methacrylic anhydride modified collagen. *China Leather* **2018**, *47*, 9−15.
(31) Chen, J.; Huang, J.; Zhang, H.; Hu, Y. A Photoresponsive Hydrogel with Enhanced Photoefficiency and the Decoupled Process of Light Activation and Shape Changing for Precise Geometric Control. *ACS Appl. Mater. Interfaces* **2020**, *12*, 38647−38654.
(32) Ganji, F.; Vasheghani-Farahani, S.; Vasheghani-Farahani, E. Theoretical Description of Hydrogel Swelling: A Review. *Iran. Polym. J.* **2010**, *19*, 375−398.
(33) Wang, W. B.; Wang, A. Q. Synthesis and swelling properties of pH-sensitive semi-IPN superabsorbent hydrogels based on sodium alginate-g-poly(sodium acrylate) and polyvinylpyrrolidone. *Carbohydr. Polym.* **2010**, *80*, 1028−1036.
(34) Kramb, R. C.; Buskohl, P. R.; Dalton, M. J.; Vaia, R. A. Belousov-Zhabotinsky Hydrogels: Relationship between Hydrogel Structure and Mechanical Response. *Chem. Mater.* **2015**, *27*, 5782−5790.
(35) Huang, Y. W.; Zeng, M.; Ren, J.; Wang, J.; Fan, L. R.; Xu, Q. Y. Preparation and swelling properties of graphene oxide/poly(acrylic acid-co-acrylamide) super-absorbent hydrogel nanocomposites. *Colloids Surf., A* **2012**, *401*, 97−106.
(36) Bueno, V. B.; Bentini, R.; Catalani, L. H.; Petri, DFS. Synthesis and swelling behavior of xanthan-based hydrogels. *Carbohydr. Polym.* **2013**, *92*, 1091−1099.
(37) Dušek, K.; Choukourov, A.; Duskova-Smrckova, M.; Biederman, H. Constrained Swelling of Polymer Networks: Characterization of Vapor-Deposited Cross-Linked Polymer Thin Films. *Macromolecules* **2014**, *47*, 4417−4427.
(38) Davidovich-Pinhas, M.; Bianco-Peled, H. A quantitative analysis of alginate swelling. *Carbohydr. Polym.* **2010**, *79*, 1020−1027.
(39) *Leather—Physical and Mechanical Tests—Determination of Thickness*, ISO 2589:2016 (IULTCS/IUP 4: 2016); International Standard, ISO: Switzerland, 2016.
(40) *Leather—Physical and Mechanical Tests—Determination of Tensile Strength and Percentage Elongation*, ISO 3376:2020 (IULTCS/IUP 6: 2020); International Standard, ISO: Switzerland, 2020.

https://doi.org/10.1021/acsomega.1c03061
ACS Omega 2021, 6, 26086−26097